DSCC2020-3309

ROLL MANEUVERABILITY OF FLAPPING FLIGHT WINGED SYSTEMS

Hamid Vejdani *

Department of Mechanical, Robotics, and Industrial Engineering
Lawrence Technological University
Southfield, Michigan 48075
Email: hvejdanin@ltu.edu

ABSTRACT

The goal of this paper is to study the effect of wing flapping kinematics on roll maneuverability of flapping flight systems. Inspired from birds maneuvering action, we study the effect of asymmetric flapping angular velocities of the wings on generating roll motions on the body. To expand the generality of the results, the equations of motion are written dimensionless. The effect of aerodynamic parameter, forward velocity and wing inertia are presented. The results show that applying asymmetric velocities during flight is useful for relatively larger wings.

Introduction

The maneuverability of flying animals and aerial vehicles is crucial for their operation in natural or urban environments. Either it is to navigate between natural obstacles like trees or construction sites, flying systems need to generate centripetal forces quickly to turn and change their trajectory sometimes to catch a prey or avoid collision. One of the common ways to generate centripetal force during flight is through generating roll angle on the body to redirect the aerodynamic force into the desired direction. Figure 1 shows examples of birds experiencing large roll angles as they fly. Generating centripetal force through roll motion is a well-known process for turning in fixed-wing airplanes (also known as banking) [1]. Airplanes generate roll angle by asymmetrically changing the angle of attack of each wing to create longitudinal torque to the body. Observations from natural fliers show birds sometimes use a different strategy to create





Figure 1. Birds' maneuver with large roll angles. Natural fliers generate roll angle for various maneuvering actions like creating centripetal force for turning. Pictures are from www.pinterest.com.

roll angle other than asymmetrically changing the wings angle of attack especially during low forward velocity. The goal of this paper is to study the effect of this bio-inspired strategy and the dynamical characteristics of the wing on the roll maneuver of flapping wing systems. The equations of motion are Non-dimensionalized to be able to expand the results regardless of the size.

Observations from avian flights during turning maneuver show that birds sometimes use asymmetric velocity on their flapping wings during flight in order to generate roll motion [2]. Figure 2 illustrates the roll creating strategy that birds use in low forward speeds. Generating roll angle is one of the well-known strategies to redirect the lift and produce centripetal force to the

^{*}Address all correspondence to this author.

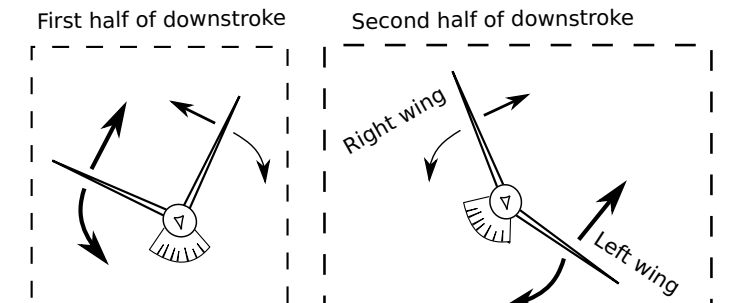


Figure 2. To create roll angle, birds move their wings asymmetrically with different velocities during down-stroke. The down-stroke starts with one wing moving at a higher angular velocity with respect to the other wing. During the second phase of the down-stroke, the velocity of the wings switch such that the momentum of the body is arrested. The straight arrows show the aerodynamic force and the curved arrows show the wing velocities [2].

center of mass trajectory for turning maneuver. Therefore, our goal is to understand the potentials of the wing kinematics in generating the roll angle.

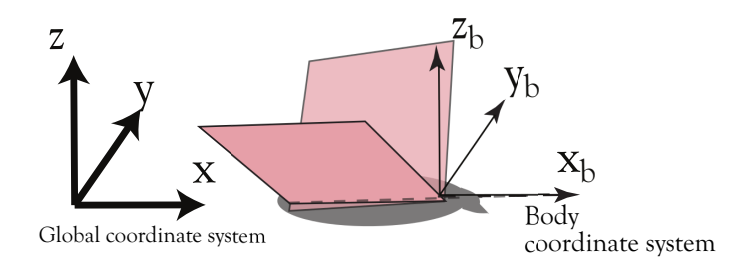
Bergou et al. [3] analyzed the bat maneuvers during landing and take off. They concluded that the wing inertia contributes dramatically to roll angle during low speed flight. In their analysis they included the flapping motion of the wings with winglength change during each wingbeat and the asymmetry was in winglength. The flapping motions of the wings in their study were assumed to be the same and therefore do not result in roll angle on the body.

Di Luca, et al. [4] created a morphing wing robot inspired from birds wing morphing during flight to enhance the maneuverability of the system. Although their focus was on aerodynamic performance of the system during flight, they showed that asymmetric morphing of the wings can enhance the roll maneuverability as well. Their paper was about fixed wing drones and therefore the flapping motions of the wings were not studied and the asymmetric wing length causes the roll motion.

Ma et al [5] studied an insect scale flapping robot for roll maneuver using the robot called RoboBee [6]. They used asymmetrical wing stroke amplitudes in generating the aerodynamic roll torques, however the results can not be generalized for larger scale systems.

Karasek et al [7] studied the rapid bank turns of insects by developing a tailless robotic flapper. They concluded that flies use torque coupling for rapid banking turns. Their focus was on insect flight and did not address roll maneuvering of larger fliers.

PerspectiveView



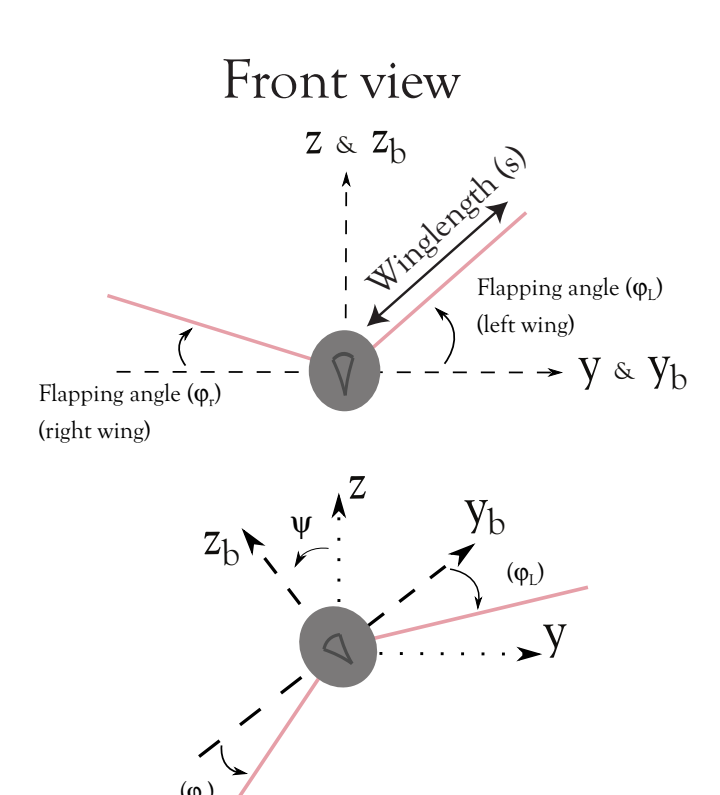


Figure 3. The model has a single roll degree of freedom (Ψ) and two flapping wings with independent degrees of freedom $(\phi_r \text{ and } \phi_L)$. The global coordinate system (x-y-z) is fixed and the body coordinate system $(x_b-y_b-z_b)$ rotates with the body. The flapping motions of the wings are with respect to the body coordinate system.

Methods

In this section the dynamical model and aerodynamic forces as well as the analysis strategy are explained.

Model

The model has a body with roll angle and two wings that each has independent flapping motion shown in figure 3. The body is a single degree of freedom that captures the effect of the wing flapping angle kinematics and wing mass distribution characteristics on roll motion.

The aerodynamics is modeled using a quasi-steady formulation implemented by a blade element method [8]. To achieve this goal, the wing is divided into finite number of stripes to calculate the aerodynamic force on the wing. Since the effective velocity of each stripe varies along the wing length, the effective angle of attack changes and therefore the integration of the aerodynamic torque is calculated numerically. For zero forward velocity, the resultant torque can be found in a closed form solution presented in other studies about hovering flight that the forward velocity is assumed zero [9, 10].

To construct the equations of motion, the Lagrangian formulation is used (L = KE - PE). Since the focus here is on the roll angle dynamics, the change in the potential energy which relates to the change in height of the center of mass can be ignored. The kinetic energy (KE) of the system is calculated by:

$$KE = \frac{1}{2}I_b\dot{\psi}^2 + \frac{1}{2}I_w(\dot{\psi} + \dot{\phi}_r)^2 + \frac{1}{2}I_w(\dot{\psi} + \dot{\phi}_l)^2$$
 (1)

Where I_b and I_w are the roll rotational inertia of the body and each wing respectively with respect to the center of the body. Using the Lagrange equation, the equations of motion can be obtained as:

$$(I_b + 2I_w)\ddot{\psi} = \tau_r + \tau_l - I_w\ddot{\phi}_r - I_w\ddot{\phi}_l \tag{2}$$

The τ_l and τ_r are the aerodynamic torques generated on the left and right wings respectively. These torques are calculated numerically at each instant of time (since they are coupled to ψ and α_e) as follows:

$$\tau_{i} = \int_{0}^{\bar{s}_{i}} \frac{1}{2} \rho \bar{c}_{i} C_{N}(\alpha_{e})_{i} (rV_{\infty}^{2} + r^{3}(\dot{\psi} + \dot{\phi}_{i})^{2}) dr, \quad i = r, l \quad (3)$$

Here, ρ , \bar{c} and \bar{s} are the air density, average wing chord and the wing length respectively. The subscript i is referred to left (l) or right (r) wing. In this equation $C_N(\alpha_e)$ is the normal aerodynamic force coefficient [9, 11] and is assumed $C_N(\alpha_e) = C_{N_0} \sin(\alpha_e)$ where $C_{N_0} = 2.0$ [3] and α_e is the effective angle of attack on each stripe that should be determined numerically based on the effective velocity at each instant of time. This

effective angle of attack is close to zero on the wing root and maximum at the wing tip in the presence of forward velocity. The effective angle of attack (α_e) varies along the wing due to the change of the flapping component of the velocity. If the free-stream velocity approaches zero (for low forward velocities), the normal coefficient approaches the drag coefficient. The direction of the torques are determined based on the sign of the total angular velocity of each wing $(\text{sign}(\dot{\psi} + \dot{\phi}_i))$.

When free-stream velocity is zero ($V_{\infty} = 0$), the integral in equation 7 can be solved analytically and the equations of motion can be written as:

$$(I_b + 2I_w)\ddot{\psi} = -\kappa((\dot{\psi} + \dot{\phi}_r)|\dot{\psi} + \dot{\phi}_r| + (\dot{\psi} + \dot{\phi}_l)|\dot{\psi} + \dot{\phi}_l| - I_w \ddot{\phi}_l - I_w \ddot{\phi}_l$$
(4)

The κ carries the size and aerodynamic properties of the wing and is defined as $\kappa = (\rho C_{N_0} \bar{c} \bar{s}^4)/8$. The non-dimensional equation of motion can be obtained by dividing both sides of the above equation by I_b as follows:

$$(1+2I^*)\ddot{\Psi} = -C^*((\dot{\Psi} + \dot{\phi}_r)|\dot{\Psi} + \dot{\phi}_r| + (\dot{\Psi} + \dot{\phi}_l)|\dot{\Psi} + \dot{\phi}_l|) - I^*\ddot{\phi}_r - I^*\ddot{\phi}_l$$

$$(5)$$

where $C^* = \kappa/I_b$ and $I^* = I_w/I_b$ are non-dimensional aerodynamic parameter and relative wing inertia respectively. These parameters reflect the effect of aerodynamic forces and wing inertia on the roll motion of the body. The advantage of rewriting the equation of motion in non-dimensional format is that it allows us to expand the generality of the outcome behavior regardless of the size of the system.

$$(1+2I^*)\ddot{\Psi} = C^*(\tau_r^* + \tau_l^*) - I^*\ddot{\varphi}_r - I^*\ddot{\varphi}_l$$
 (6)

Where the corresponding torques can be calculated as:

$$\tau_i^* = \int_0^1 4\sin(\alpha_e)_i (\xi(\frac{V_\infty}{\bar{s}})^2 + \xi^3(\dot{\psi} + \dot{\phi}_i)^2) d\xi, \ i = r, l \quad (7)$$

Analysis

The analysis starts from the beginning of the down-stroke (t = 0) and ends when the wings reach the designated flapping angles $(t = t_f)$. The relative angular velocity of the wings with respect to the body are zero at the beginning and end of the down-stroke $(\dot{\phi}_i(0) = \dot{\phi}_i(t_f) = 0, i = L, r)$. While the two wings share the same instant for starting and ending the down-stroke (t = 0)

wings at the beginning of downstroke (t=0) Flapping angle range

 $\Delta \phi_{
m r}$

range

wings at the end of downstroke $(t=t_f)$

Figure 4. The angle that each wing sweeps (flapping angle range) during the maneuvering down-stroke ($\Delta \phi_r$ and $\Delta \phi_L$).

and $t = t_f$), the instances at which the angular accelerations of the wings change, can be different (t_{r1}, t_{L1}) in figure 5) as well as the maximum flapping angular velocity $(\dot{\varphi}_L(t_{L1}))$ and $\dot{\varphi}_r(t_{r1})$ that wings reach during the down-stroke. Therefore, the angle that each wing sweeps during the down-stroke $(\Delta \varphi_L)$ and $\Delta \varphi_r$ in figure 4) can be determined as follows:

$$\Delta \phi_L = \phi_{Lf} - \phi_{L0}, \quad \Delta \phi_r = \phi_{rf} - \phi_{r0}$$

Given these sweeping angles, and the time history of the flapping motions, the maximum angular velocity and accelerations of the wings can be calculated.

Since in this study we are interested in those wing flapping kinematics that lead to zero roll momentum at the end of the down-stroke ($\psi(t_f)=0$) we search for only those combinations of sweeping angles and internal critical times (t_{L1} and t_{r1}) that result in zero roll momentum at the end of the down-stroke. The continuity of the functions for wing kinematics are chosen such that they can be implemented on a robotic platform. These flapping kinematics are shown in figure 5.

Results and discussion

We start the result with presenting an example of the wing flapping motion that results in body roll rotation with zero momentum at the end of the down-stroke. Figure 6 shows the body roll angle and angular velocity caused by the wings' flapping motion at zero forward velocity ($V_{\infty} = 0$). As inspired from birds roll motion (figure 2), one wing starts the down-stroke with higher velocity than the other one and they reverse the course during the down-stroke to arrest the roll momentum created on the body. In this figure, the time is normalized based on the final time (t_f).

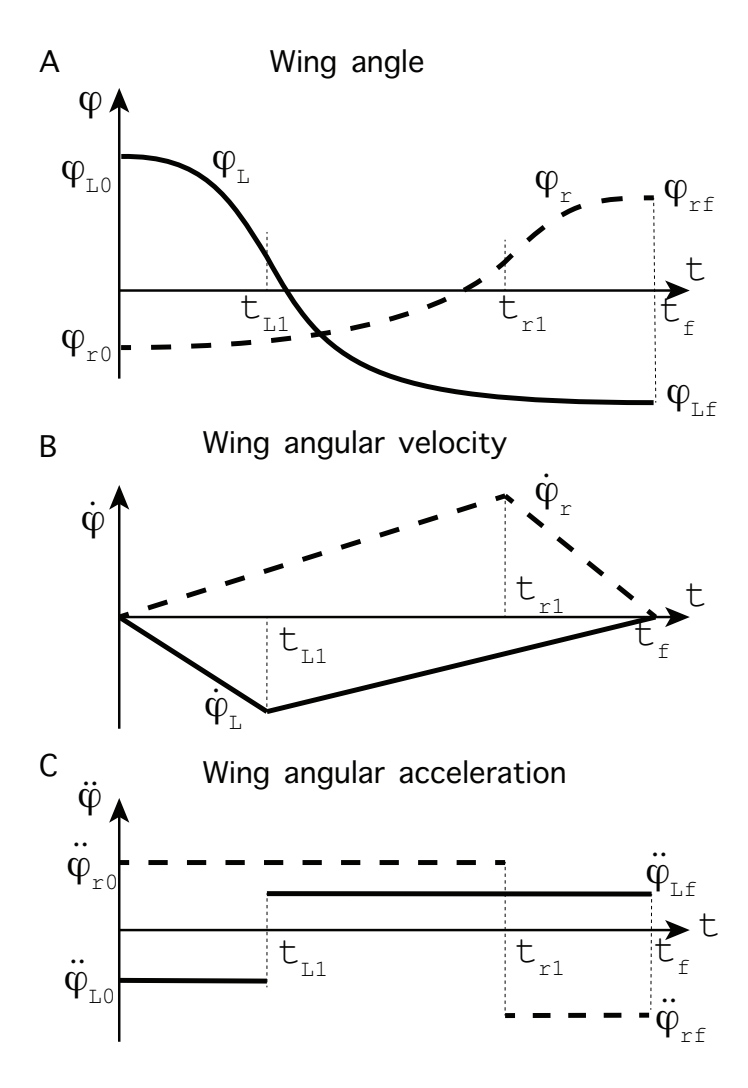


Figure 5. The kinematics of wings (A) flapping angle, (B) angular velocity, and (C) angular acceleration during a down-stroke. The angle that each wing sweeps during the down-stroke is $\Delta \phi_i = \phi_{if} - \phi_{i0}$, i = L, r.

For this example the relative inertia of the wings is zero ($I^* = 0$) and the aerodynamic parameter is $C^* = 1$.

Figure 7 presents all the solutions that can be obtained with the wings sweeping all the possible flapping angles ($\Delta \phi_r$ and $\Delta \phi_l$). It is assumed that $\Delta \phi_{r,l} < 160^\circ$ as physical limitation for wings to sweep as flapping motion (figure 4). The contour lines in figure 7 are the magnitude of the body roll rotation at the end of the down-stroke. The grey region shows where the solution can not be found because the body momentum can not be arrested at the end of the down-stroke. All the possible solutions are in the region between the 45° (symmetry) line and the start of the grey region. It should be noted that due to the symmetry of the wings motion on the 45° line, the body experiences zero roll motion on this line. The body experiences counterclockwise

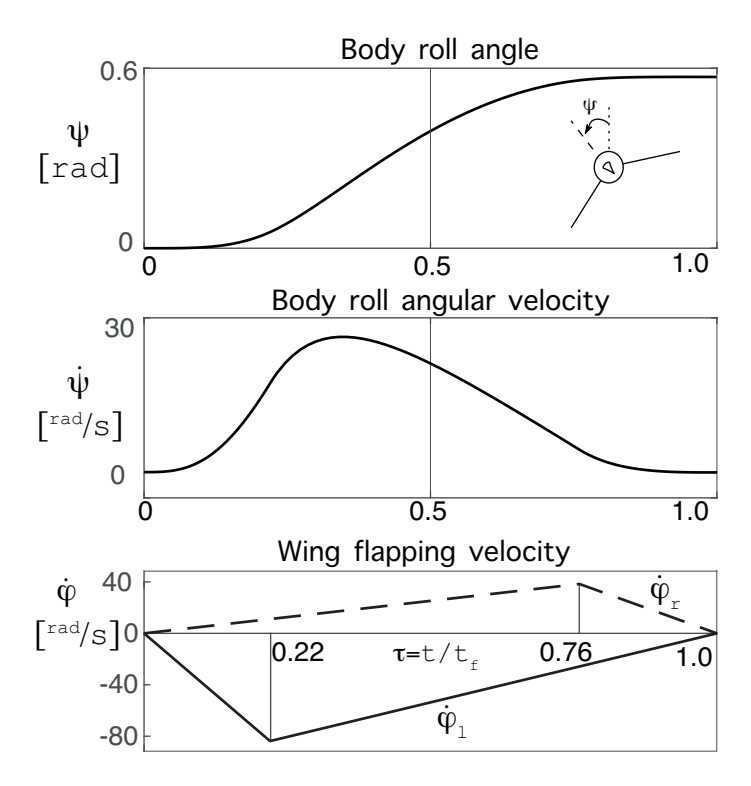


Figure 6. An example of wing flapping motion and its effect on the roll rotation and velocity of the body. To obtain a net roll angle with zero momentum at the end of the down-stroke, the left wing moves faster in the beginning and then slows down while the right wing starts with a lower velocity and then moves faster to arrest the momentum of the body. At the end of the down-stroke, both wings reach zero velocity along with the body.

wise rotation bellow the symmetry line and negative roll motion above this line. Since the body roll angle increases as the contour lines get further from the 45° line, to achieve higher roll angle, the region between the symmetry line and the grey region should be expanded. In this figure, the maximum roll angle is about 65° which is at the furthest distance to the symmetry line.

The effect of non-dimensional aerodynamic parameter (C^*) on the roll angle is shown in figures 8 and 9 for $V_{\infty}=0$ and $V_{\infty}=5~m/s$ respectively. Like before, the region between the 45° line and each grey boundary shows the possible solution region. Comparing these two figures to each other shows the forward velocity expands the solution region and therefore gives higher roll angle at the end of the down-stroke. Moreover, both figures show that increasing C^* expands the solution region regardless of the forward velocity. Therefore, for systems with small C^* (like flies with about $C^* < 0.1$ [3]) the roll rotation is small and not practical to use this body roll generating strategy while for birds' and bats' scale $C^* > 0.5$ [3] and this strategy is useful.

Figure 10 shows the effect of wing inertia on the body roll

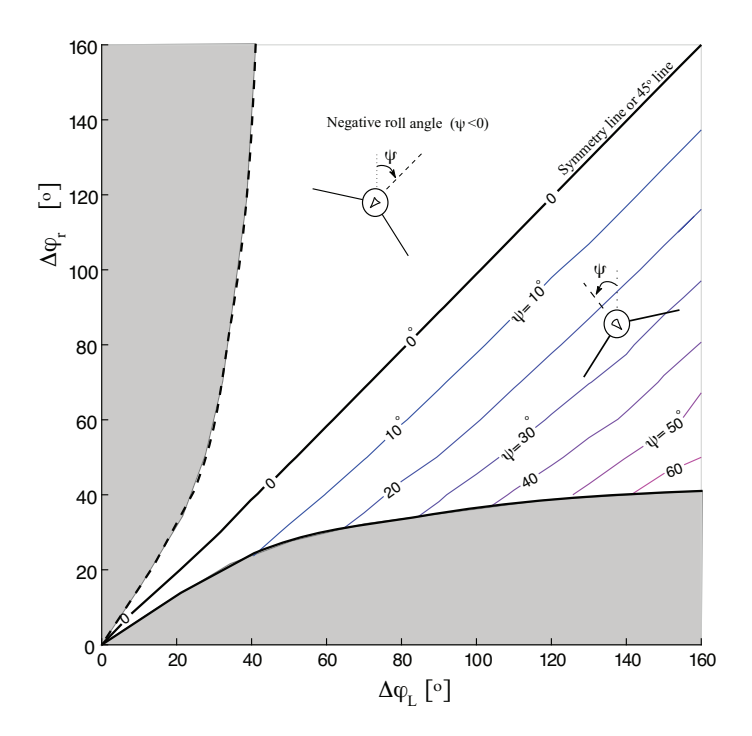


Figure 7. The effect of asymmetric wing motion on the body roll angle. In the grey regions solution can not be found (the body roll momentum can not be arrested at the end of the down-stroke). If the wings move symmetrically, the solution will be on the 45° (symmetry) line. Positive (counterclockwise) roll angles are between below the symmetry line until the grey region boundary. Negative (clockwise) roll angles are above the symmetry line until the grey region boundary.

angle in zero forward velocity ($V_{\infty}=0$). In this figure the aero-dynamic parameter is assumed $C^*=1$. The possible solution region between the 45° line and the grey boundaries expand as the relative wing inertia decreases. While for insect scale systems I^* is close to zero, but since C^* is close to zero as well, the system can not achieve acceptable roll angle. This figure shows that birds with relatively lower I^* with respect to bats have a better performance in using this body roll generating strategy.

Conclusion

In this paper a bio-inspired strategy to create roll motion on flapping wing flight systems is studied. The strategy is based on creating asymmetric velocity on the wings during a downstroke. The results showed that for relatively large wings and low wing mass with respect to the body inertia, the system can experience large roll angle after only a down-stroke. As the wing inertia increases, the resultant roll angle at the end of the downstroke decreases which suggests the deficiency of this strategy for heavy wing systems like bats. The overall results show for systems with large aerodynamic parameter and low wing inertia

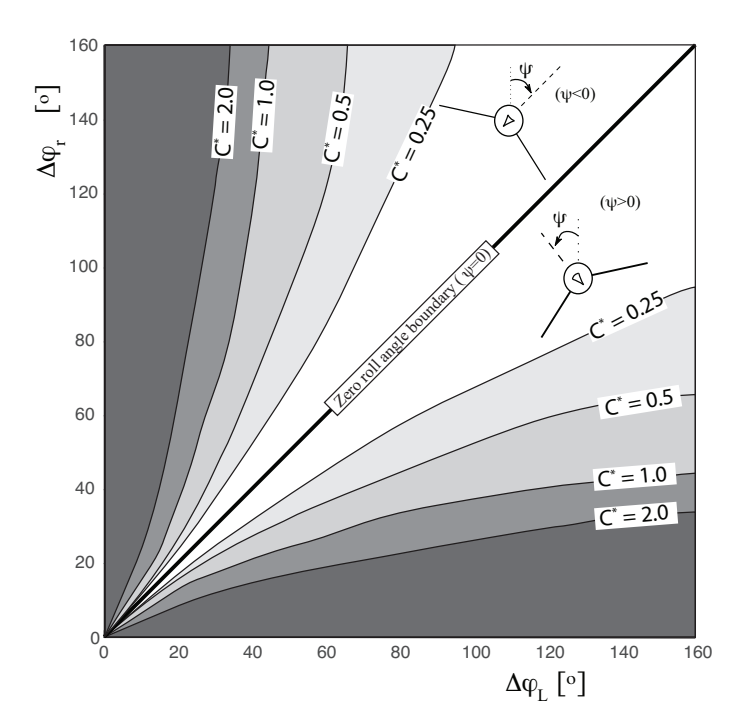


Figure 8. The effect of aerodynamic parameter (C^*) on the roll angle for systems with zero forward velocity ($V_\infty=0$) and massless wings ($I^*=0$). The solution region (between the 45° line and each grey region boundary) expands as C^* increases.

(like birds in general), this strategy can be useful as it is used by birds in nature.

FUTURE WORK

Implementation of the findings in this paper on a single degree of freedom robotic prototype is the next step to compare the results. After that the model will be expanded and the interactions of other degrees of freedom will be studied.

ACKNOWLEDGMENT

This study was funded by grant number 1931122 from the National Science Foundation (NSF).

REFERENCES

- [1] Kermode, A. (2011), Mechanics of Flight, Prentice Hall.
- [2] Tobalske, B. W. (2007), Biomechanics of bird flight, *Journal of Experimental Biology* **210**, 3135–3146.
- [3] Bergou, A. J., Swartz, S. M., Vejdani, H., Riskin, D. K., Reimnitz, L., Taubin, G., and Breuer, K. S. (2015), Falling with style: Bats perform complex aerial rotations by adjusting wing inertia, *PLoS Biol* 13, 1-16.

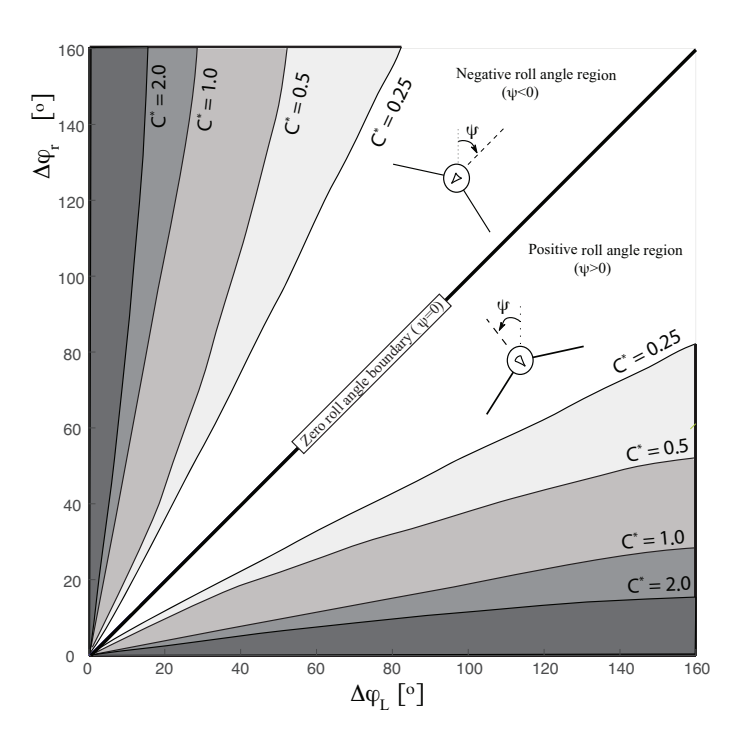


Figure 9. The effect of C^* on the roll angle of the body with $V_\infty=5$ and massless wings ($I^*=0$). As the C^* increases, the region that the roll angle exists expands (the region between the 45° line and the boundary of each grey region). If the wings move symmetrically, the 45° line is obtained which means zero roll angle ($\Psi=0$) at the end of the downstroke.

- [4] Di Luca, M., Mintchev, S., Heitz, G., Noca, F., and Floreano, D. (2017), Bioinspired morphing wings for extended flight envelope and roll control of small drones, *Interface Focus* 7, 20160092.
- [5] Ma, K. Y., Chirarattananon, P., Fuller, S. B., and Wood, R. J. (2013), Controlled flight of a biologically inspired, insect-scale robot, *Science*.
- [6] Wood, R. J. (2008), The first takeoff of a biologically inspired at-scale robotic insect, *IEEE Transactions on Robotics* 24, 341-347.
- [7] Karásek, M., Muijres, F. T., De Wagter, C., Remes, B. D. W., and de Croon, G. C. H. E. (2018), A tailless aerial robotic flapper reveals that flies use torque coupling in rapid banked turns, *Science* 361, 1089–1094.
- [8] Sane, S. P. and Dickinson, M. H. (2002), The aerodynamic effects of wing rotation and a revised quasi-steady model of flapping flight, *Journal of Experimental Biology* 205, 1087–1096.
- [9] Byl, K. (2010), A passive dynamic approach for flapping-wing micro-aerial vehicle control, volume ASME 2010 Dynamic Systems and Control Conference, Volume 1 of *Dynamic Systems and Control Conference*. pp. 215–223.

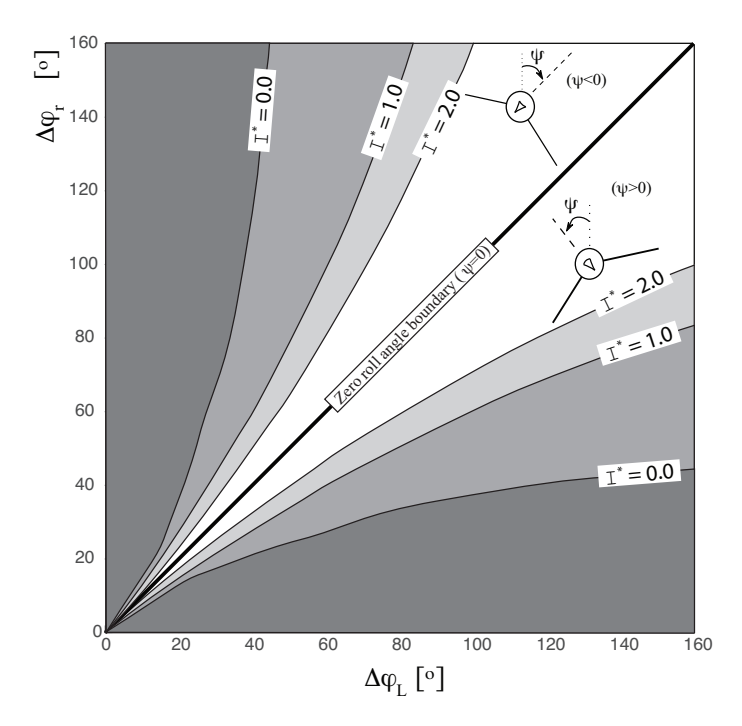


Figure 10. The effect of wing inertia on the body roll motion. Here, the forward velocity is zero $(V_\infty=0)$ and $C^*=1$. Below the 45° line shows positive roll angle $(\Psi>0)$ and above this line shows the negative roll angle $(\Psi<0)$. Solutions exist in the region bounded from the 45° line until the the associated grey regions (based on I^*). The grey regions show where the solution does not exist. As the wing inertia increases, the solution region expands and therefore the body can experience higher roll rotation at the end of the down-stroke.

- [10] Kruyt, J. W., Quicazán-Rubio, E. M., van Heijst, G. F., Altshuler, D. L., and Lentink, D. (2014), Hummingbird wing efficacy depends on aspect ratio and compares with helicopter rotors, *Journal of The Royal Society Interface* 11.
- [11] Cheng, B. and Deng, X. (2011), Translational and rotational damping of flapping flight and its dynamics and stability at hovering, *IEEE Transactions on Robotics* **27**, 849-864.